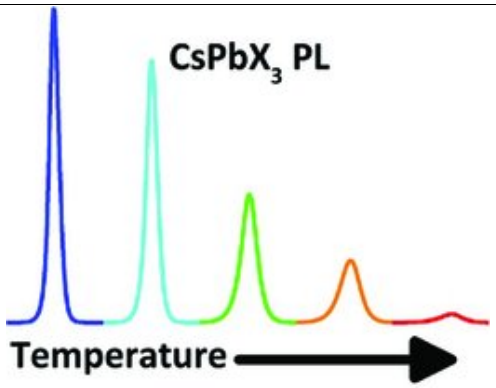

High-temperature photoluminescence properties of $CsPbX_3$ nanocrystals are important to the viability of this family of emitters in lighting and display applications. The persistence of photoluminescence at temperatures above 400 K depends strongly on the halide composition, and photoluminescence loss occurs through thermally assisted trapping to halogen vacancies.

High-Temperature Photoluminescence of $CsPbX_3$ (X = Cl, Br, I) Nanocrystals

By Benjamin T. Diroll[1], Georgian Nedelcu[2], Maksym V. Kovalenko[2,3] and Richard D. Schaller[1,4,*]

[1]Dr. B. T. Diroll, Prof. R. D. Schaller, Center for Nanoscale Materials, Argonne National Laboratory, Lemont, IL, 60439, USA

[2]G. Nedelcu, Prof. M. V. Kovalenko, Department of Chemistry and Applied Bioscience, ETH Zürich, Vladimir Prelog Weg 1, CH-8093, Zürich, Switzerland

[3]Prof. M. V. Kovalenko, Empa – Swiss Federal Laboratories for Materials Science and Technology, Überlandstrasse 129, CH-8600, Dübendorf, Switzerland

[4]Prof. R. D. Schaller, Department of Chemistry, Northwestern University, Evanston, IL, 60208, USA

*Correspondence to: Prof. R. D. Schaller (E-mail: schaller@anl.gov) Q1: [APT to AU][Please provide the highest academic title (either Dr. or Prof.) for all authors, where

applicable.]

Received: 2016-12-21, Revised: 2017-02-15, Online: YYYY-MM-DD

Recent synthetic developments have generated intense interest in the use of cesium lead halide perovskite nanocrystals for light-emitting applications. This work presents the photoluminescence (PL) of cesium lead halide perovskite nanocrystals with tunable halide composition recorded as function of temperature from 80 to 550 K. $CsPbBr_3$ nanocrystals show the highest resilience to temperature while chloride-containing samples show relatively poorer preservation of photoluminescence at elevated temperatures. Thermal cycling experiments show that PL loss of $CsPbBr_3$ is largely reversible at temperatures below 450 K, but shows irreversible degradation at higher temperatures. Time-resolved measurements of $CsPbX_3$ samples show an increase in the PL lifetime with temperature elevation, consistent with exciton fission to form free carriers, followed by a decrease in the apparent PL lifetime due to trapping. PL persistence measurements and time-resolved spectroscopies implicate thermally assisted trapping, most likely to halogen vacancy traps, as the mechanism of reversible PL loss.

Keywords

$CsPbX_3$, high-temperature, perovskites, photoluminescence, stability

1 Introduction

The tremendous success of organolead halide perovskites for photovoltaic cells[1] and other optoelectronic applications[2,3] demonstrated in the last five years has led to intense exploration of related chemistries.[4,5] Among the most promising reported materials for light-emitting applications in the visible spectrum are the cesium lead halide perovskite analogues ($CsPbX_3$), in which the organic cation is replaced by cesium.[6,7] By tuning the halide composition of these materials, the photoluminescence can be tuned through virtually the whole visible spectrum. As colloidal nanocrystals (NCs), these materials have emission with high quantum yield and high color purity[8] which have been used in light-emitting devices such as low-threshold lasers,[9,10] light-emitting diodes (LEDs),[11,12,13,14,15] and downconverting layers[16,17,18] similar to those used in quantum dot display technology. Survival of advantageous properties at high temperature, which is a significant problem for organolead halide perovskites,[19,20] is one challenge to the use of such NCs in many of these technologies, which require stable materials at temperatures often exceeding 100 °C.

This work studies the photoluminescence (PL) of $CsPbX_3$ NCs of variable halide composition from 80 K to up to 550 K. The PL intensity of the NC samples decreases with temperature elevation, decreasing to intensities less than 0.1% of the initial PL as measured at 80 K. However, the resilience of PL at temperatures below 450 K is strongly dependent on the halide composition of the NCs.

Chloride-containing NCs show consistently greater susceptibility to thermal quenching than pure bromide, iodide, or iodide-bromide-mixed halides. Pure $CsPbBr_3$ NCs show the greatest thermal stability among the samples measured, with bromide-iodide and pure iodide compounds substantially more stable than chloride-containing NCs. However, PL persistence is considerably lower than other reported NCs—typically core/shells—proposed for optoelectronic technologies. Most $CsPbX_3$ NCs display small blueshifts with increasing temperature and each display increased sensitivity of thermal broadening compared to other visible NC emitters.

Experiments on reversibility of PL loss of $CsPbBr_3$ NCs implicate both reversible (to 450 K) and irreversible (>450 K) loss pathways. Irreversible loss corresponds to ligand desorption, supported by thermogravimetric analysis (TGA) measurements, and underscores the substantial advantages of any potential core/shell structure. Examination of several sizes of $CsPbBr_3$ NCs suggests that reversible PL loss most likely arises from thermally activated trapping into halogen vacancies. Time-resolved PL data show that for $CsPbX_3$ NCs, the intrinsic radiative rate decreases with temperature elevation, due to exciton fission, up to a threshold value at which the apparent lifetime of PL and transient absorption (TA) decreases due to thermally assisted carrier trapping at halogen vacancies.

2 Temperature Dependence of Steady-State Photoluminescence of $CsPbX_3$ Nanocrystals

Figure 1 shows transmission electron microscopy (TEM) images and optical spectra of the samples used in this work. Unlike quantum dots such as CdSe, tunable emission throughout the visible spectrum does not accompany major changes in the particle size. The samples range in size from 9 to 13 nm and all formed predominantly into NCs of cubic morphology. The composition of the samples is varied by changing the lead halide precursors used in the synthesis (e.g., synthesis of $CsPbBrI_2$ used 67 mol% PbI_2 and 33 mol% $PbBr_2$) and tuning the reaction temperature to obtain similar sized NCs. Each of the seven samples progressively changes the composition by one halide ion, varying the PL energy of the samples at room temperature from 3.05 eV for pure $CsPbCl_3$ to 1.75 eV for pure $CsPbI_3$. Q2: [APT to AU][Please check that the edits to the preceding sentence are OK and that the meaning has not been changed.]

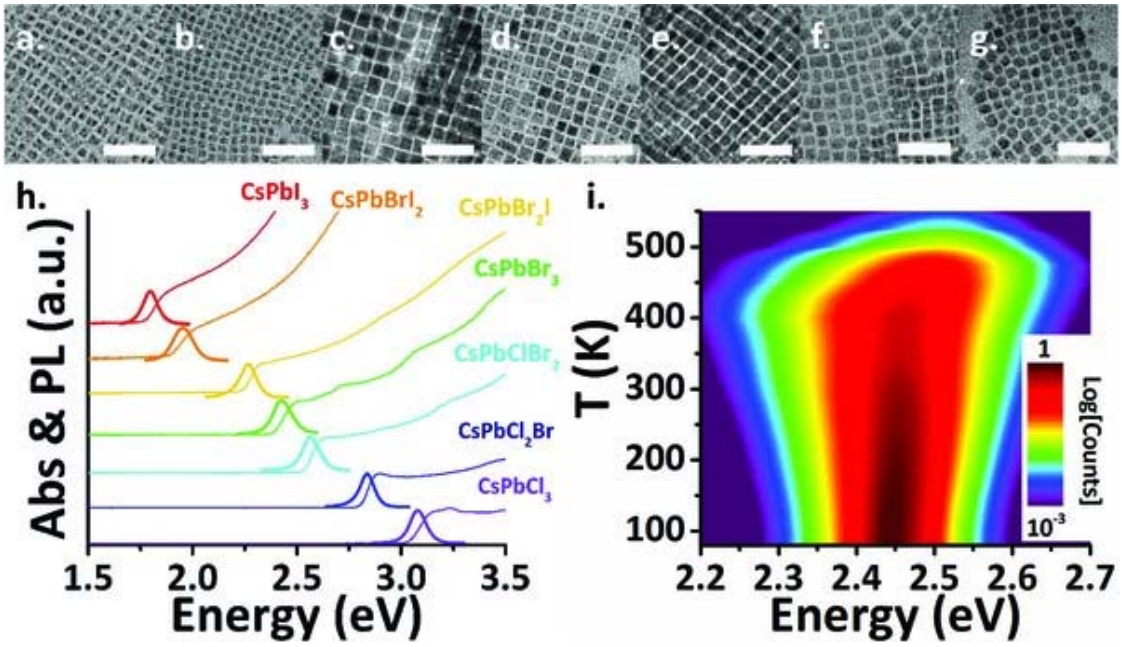

Figure 1 TEM images of $CsPbX_3$ perovskite NCs: a) $CsPbCl_3$, b) $CsPbCl_2Br$, c) $CsPbClBr_2$, d) $CsPbBr_3$, e) $CsPbBr_2I$, f) $CsPbBrI_2$, and g) $CsPbI_3$. Scale bars in images (a)–(g) represent 50 nm. h) Absorption spectra (thin lines) and PL spectra (thick lines) of $CsPbX_3$ samples. i) 2D map showing the PL intensity of a $CsPbBr_3$ NC sample plotted against temperature and energy. The color map is on a logarithmic scale. Q3: [APT to AU][If you have not returned the color cost confirmation form already, please email the completed form to the editorial office when you submit your proof corrections. This will confirm that you are willing to support the cost for color publication of the figures. Details about our color policies and a link to the form were included with your acceptance email. If you wish for your figures to be presented in greyscale, please email the editorial office to confirm this.]

A typical example of the high-temperature PL measurement is plotted in Figure 1i, showing the emission of a $CsPbBr_3$ sample as a function of emission energy and temperature. Like all other examples in this work, the NC sample was embedded into a polymer host to reduce inter-NC interactions which may diminish PL intensity and mimic the form of use in NC-based displays (see the Experimental Section and Figure S1, Supporting Information, for more details). Certain qualitative features are noteworthy in the PL data shown in Figure 1i. First, the emission intensity, which is plotted on a logarithmic scale, decreases subtly to 450 K and then drops dramatically lower for temperatures exceeding 450 K. Second, the emission energy of the sample blueshifts with higher temperatures, indicating that the band gap of the $CsPbBr_3$ increases, behavior which is also observed in related halide perovskites,[21,22,23] but the opposite of behavior of IV, III–V, and II–VI semiconductors.[24] Third, the bandwidth of the PL, a critical parameter for enhanced color gamut, broadens at high temperature.

A quantitative analysis of the temperature-dependent PL of each sample appears in **Figure 2**. Figure 2a plots the integrated PL of the samples normalized to the measured emission at 80 K. Although PL of each of the samples decreases to $\approx 10^{-3}$ or lower for >500 K, the chloride-containing samples showed markedly lower preservation of PL at intermediate temperatures, a fact emphasized in the inset in Figure 2a. These samples show the onset of a steep decline in PL beginning near 300 K, whereas samples that do not contain chloride ions decrease dramatically closer to 375 K and above,

with the $CsPbBr_3$ sample showing the greatest preservation of PL at nearly all measured temperatures.

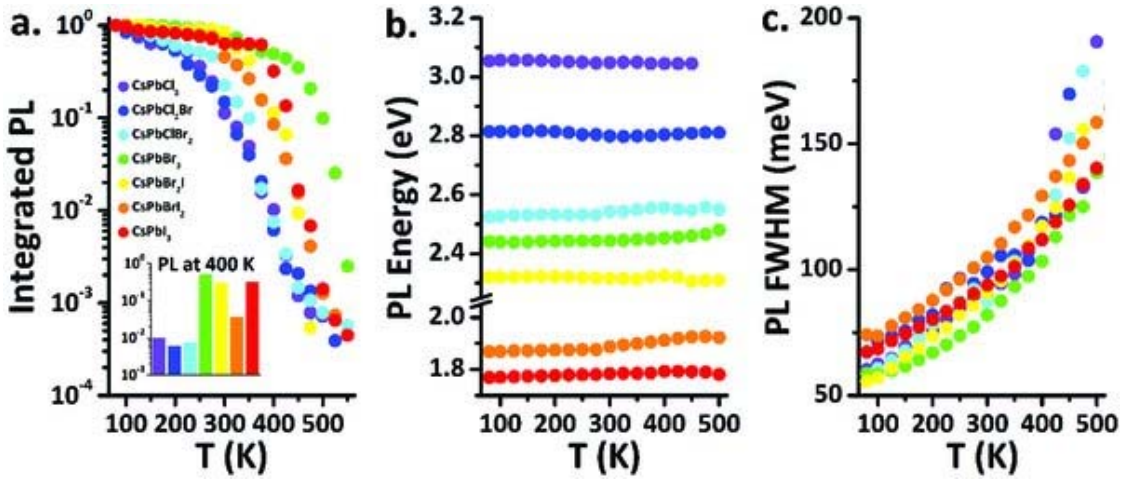

Figure 2 a) Integrated PL of $CsPbX_3$ NC samples plotted versus measurement temperature. The inset bar plot shows the fraction of emission (relative to 80 K) of each sample at 400 K, in corresponding colors. b) Emission peak center energy of the $CsPbX_3$ samples versus temperature. c) Temperature-dependent PL bandwidth measured from the full-width at half maximum (FWHM) of the $CsPbX_3$ samples.

It is also worth comparing these results to some of the results previously published in the literature on similar materials, primarily at lower temperature ranges. Compared to organolead halide perovskites, Cs-based lead trihalide perovskites are known to substantially higher stability under most environmental conditions.[25,26,27] Single crystals of Cs-based plumbotrihalides have, for example, demonstrated thermal stability to 600 °C, whereas organolead halide perovskites become unstable near 300 °C.[25] Indeed, bulk organolead halide perovskites show near complete loss of PL when heating from 300 to 400 K, although quantum dots of the same preserve ≈30% of PL over the same temperature range comparable to our samples.[22] $CsPbBr_3$ NCs synthesized at room temperature in DMF/toluene mixtures show substantial (≈85%) PL loss upon heating from 80 to 273 K,[11] compared to losses reported here of less than 10% for the same composition over a similar temperature range. Similar materials also made at room temperature showed PL losses of up to 80% upon heating above room temperature to 373 K.[28] In a related work, $CsPbBr_3$ and $CsPbCl_3$ single crystals grown by the Bridgman technique are also reported to show relatively poorer PL persistence at low temperature, with PL decreasing by more than 90% when heating samples from 10 to 180 K.[29] Later in this work, we will address a series of experiments which explore the origins of PL loss in $CsPbX_3$ NC samples.

To obtain the emission energy and linewidth, Voight fits were applied to the PL data for each of the samples. As the PL becomes very weak for the highest measured temperatures, fitting data from those points with less than 0.1% of the original PL intensity were excluded. Q4: [APT to AU][Please check that the edits to the preceding sentence are OK and that the meaning has not been changed.] Figure 2b shows that like the $CsPbBr_3$ samples in Figure 1i, PL energy blueshifts slightly (less than 25 meV) with elevated temperature for most samples. This behavior is unusual; for comparison, CdSe NCs redshift by 100 meV over same measured temperature range. On the other hand, in some cases in Figure 2b, the PL energy barely changes at all and reports on $CsPbX_3$ materials

have yielded similarly mixed results.[30] A Varshni relation of the form $E_{gap}(T) = E_{gap}(0) - \alpha T^2/(\beta + T)$[24] was used to fit the PL data with the fit parameters reported in Table S1 (Supporting Information). Varshni fits of the PL data yield an α parameter which ranges from -1.9×10^{-4} to 3.7×10^{-5} K^{-1} for the samples. In addition to being negative for most samples indicating a blueshift, this represents a smaller wavelength shift with temperature than found for most semiconductors[24] and consistent with previous reports which claim small shift of PL energy of $CsPbBr_3$ NCs from 25 to 100 °C.[31] The β parameter obtained from Varshni fits, which in principle corresponds to the Debye temperature,[24] is ≈300 K for most of the $CsPbX_3$ NCs.

The bandwidth of PL for all of the samples varies with temperature in a similar manner, as shown in Figure 2c, in each case presenting <75 meV linewidth at 80 K. Thermal broadening of PL increases linearly on acoustic phonon–exciton coupling and nonlinearly based on longitudinal optical (LO) phonon–exciton coupling.[32,33] The nonlinear increase in the PL linewidth with elevated temperature is evidence for the contribution of both acoustic and optical phonons in the thermal broadening. Raman spectra of $CsPbX_3$ samples indicate a complex manifold of LO phonons which may contribute to the broadening of PL spectra at higher temperatures.[34,35] Data in Figure 2c indicate that PL broadening in $CsPbX_3$ is significantly more temperature-sensitive than for II–VI NCs, especially above 300 K.[32,36,37,38,39] For example, the $CsPbBr_3$ sample broadens from 82 meV at 300 K to 139 meV at 500 K (+70%), whereas CdSe/CdS NCs show an increase of full width at half maximum (FWHM) from 87 to 96 meV (+10%) over the same temperature range.[36] As a practical matter, this means that temperature elevation of $CsPbX_3$ reduces achievable color gamut more than II–VI materials, although the wavelength of the emission appears relatively more stable.

3 Mechanisms of Photoluminescence Loss

To determine the cause of PL loss with temperature elevation, several experiments were performed. Cyclic heating experiments disambiguate loss of PL due to reversible and irreversible processes. **Figure 3** shows the results of multiple heating and cooling steps for a $CsPbBr_3$ sample normalized to the PL intensity at 300 K. Cooling samples below 300 K increased the PL, as shown in Figure 2a, but the integrated intensity was the same when returning to 300 K, indicating full reversibility of PL loss up to room temperature. Figure 3 shows that PL loss upon heating to 400 K is reversible to >95% of the intensity at 300 K and PL loss to 450 K is >80% reversible. Previous works have also shown substantially reversible PL losses in samples heated from room temperature to 373 K.[28] Only upon heating the sample above 450 K does PL loss becomes mostly irreversible. The onset of substantial irreversible PL loss occurs at the same temperatures where the integrated PL intensity drops rapidly with increasing temperature for $CsPbBr_3$ samples.

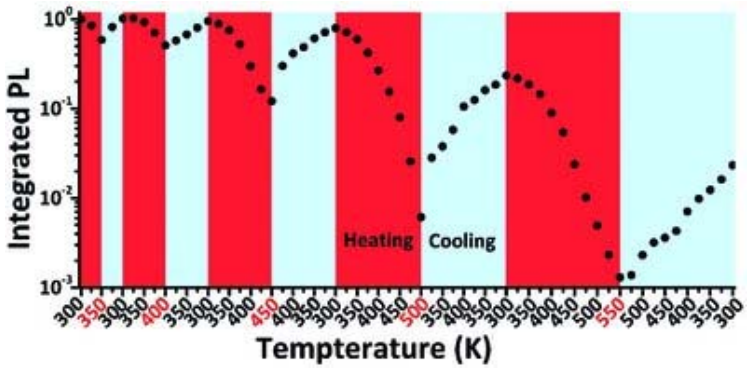

Figure 3 Thermal cycling measurements of $CsPbBr_3$ PL. High set point temperatures are highlighted in red for clarity.

Time-resolved emission and transient absorption measurements collected at different heating temperatures provide additional insight into PL loss pathways and support a thermally assisted trapping model. Figure 4a shows the time-resolved photoluminescence (TRPL) of a $CsPbBr_3$ sample (≈200 ps time resolution), which shows an increase in the PL lifetime from 80 to 450 K, whereupon the lifetime decreases rapidly, corresponding to the precipitous loss of PL intensity. A similar hump-shaped TRPL signal has been observed previously in CdSe/CdS heterostructures,[36,40] but represents another unusual feature of $CsPbX_3$ NCs. Core-only CdSe, Si, and InP NCs all show a monotonic decrease in PL lifetime with heating.

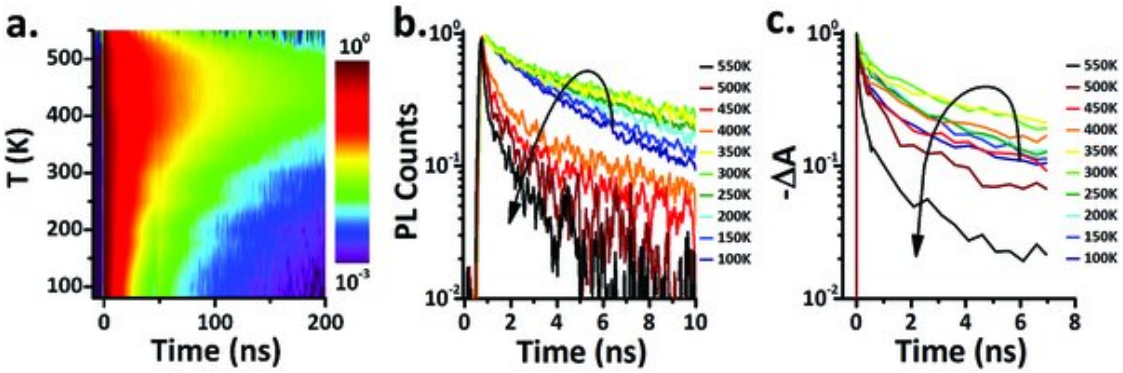

Figure 4 a) 2D map of PL of $CsPbBr_3$ NCs plotted against temperature and time collected using an avalanche photodiode. The color scale is logarithmic and data are normalized to the maximum at each temperature. b) Normalized streak camera TRPL traces as a function of temperature for the same $CsPbBr_3$ NCs. c) Normalized transient absorption traces of the band-edge bleaching feature of the same $CsPbBr_3$ NCs.

To confirm this trend and analyze temperature-dependent recombination of excitons with higher time resolution, we performed ultrafast TRPL measurements and transient absorption (TA). Careful comparison of TRPL and TA data of III–V and II–VI NCs allows discrimination of electron and hole trapping behavior.[41,42] However, disambiguating the cause of decreased PL with temperature in $CsPbX_3$ NCs is a challenge, because the effective masses of electrons and holes in this composition are very similar.[6,43] Because both carriers have potential to generate a similar bleach feature in TA, the ultrafast TRPL and TA signals are expected to be similar, which is what we indeed find in Figure 4b,c. This means that we cannot distinguish if trapping is unipolar or which carrier is trapped. However, ultrafast measurements recapitulate the pattern observed in Figure 4a: as the temperature is raised, the

TRPL and TA signals show an increase in the decay time up to a threshold temperature (here 400 K), after which the decay time decreases. The discrepancy in the apparent threshold temperature is most likely due to differences in the time resolution of the experiments.

All sets of time-resolved data on $CsPbBr_3$ show an initial increase in the lifetime followed by a substantial decrease in carrier lifetime above a threshold temperature, with the excited-state lifetime becoming comparatively brief (<1 ns) at the highest temperatures measured. Although the focus here is on a $CsPbBr_3$ sample, $CsPbCl_3$ and $CsPbI_3$ show substantially similar behavior in time-resolved measurements (Figure S3, Supporting Information). Time-resolved data are interpreted to show a decrease in the intrinsic radiative rate for $CsPbBr_3$ with increasing temperature, followed, above a threshold temperature, by the increasing presence of nonradiative pathways for recombination, first to reversibly occupied trap states and then to irreversible PL loss. Previous work has identified fission of bound excitons, with an energy of 40–50 meV as the cause for weaker PL at higher temperatures in $CsPbBr_3$ NCs.[7,11,39] The increased energy available for separation of excitons is consistent with the increase in the apparent lifetime, wherein free carriers recombine more slowly than bound excitons resulting in delayed fluorescence. Although it has been implicated in the higher PL of perovskite quantum dots versus bulk materials,[22,44,45] exciton separation is not, by itself, an explanation for decreased PL, which requires nonradiative decay pathways.

To identify possible nonradiative decay pathways responsible for reversible and irreversible PL loss, a series of size-dependent measurements were performed using $CsPbBr_3$ NCs. Although the NC size does not substantially change the emission energy at the size range measured for the $CsPbX_3$ NCs described above, it may still yield effects on thermal stability. Several sizes of $CsPbBr_3$ NCs were measured with the results shown in **Figure 5**a. Among the samples which range from 7.1 to 11.0 nm (400% change in volume), there is no systematic difference in the PL properties with size, with each sample exhibiting substantially similar thermal stability. This strongly suggests that both reversible and irreversible PL loss mechanisms are independent of the size of the NCs over the range examined in this work.

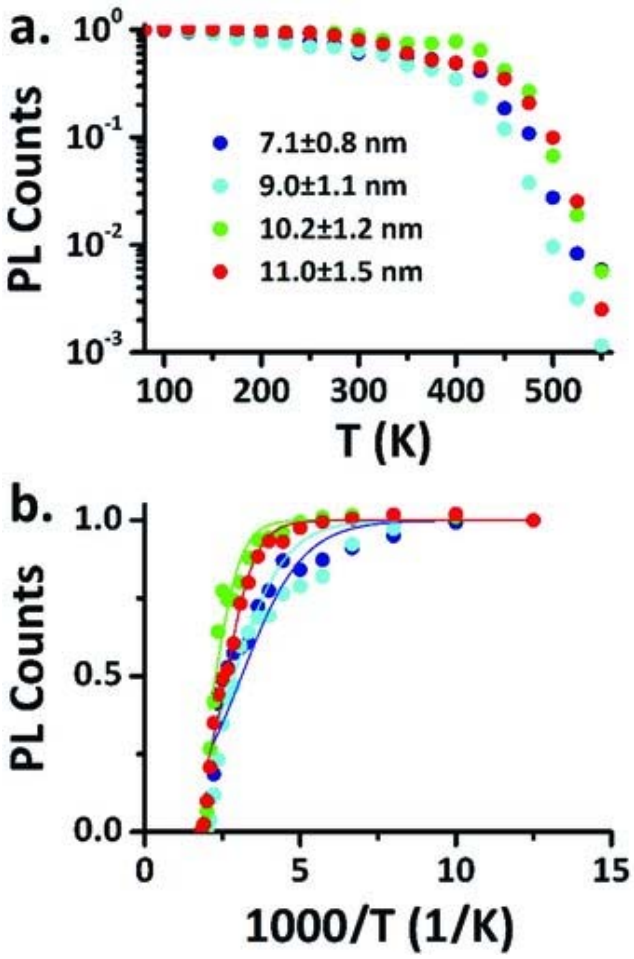

Figure 5 a) Integrated PL of several sizes of $CsPbBr_3$ NCs measured as a function of temperature. b) Fitting of PL decay of $CsPbBr_3$ samples to a single reversible trap state model.

From thermal cycling experiments described above and shown in Figure 3, irreversible PL losses dominate when the $CsPbBr_3$ samples are heated above 450 K. Thermal analysis of $CsPbBr_3$ NCs (Figure S4, Supporting Information), which show a large weight loss around 425 K, supports the argument that irreversible PL loss is related to loss of organic ligands on the NC surface.[40] In the case of $CsPbX_3$ NCs, the ligand shell is composed of both carboxylate and amine ligands bound to cationic and anionic sites, in contrast to the metal-rich surfaces of most semiconductor nanocrystals,[48] and desorption or alteration of either could yield irreversible PL loss. This may be due to both the loss of electronic passivation and surface traps, as has been found in CdSe[40] and InP,[46] but can also arise from structural changes which also occur at elevated temperatures and are enabled by dynamic ligand coverage. X-ray diffraction data (Figure S5, Supporting Information) show that heating to 500 K induces sintering in dense films of NCs, but not in films of well-separated NCs embedded in a polymer, such as those used in our studies.[16,47] Therefore, consistent with thermal analysis data, X-ray diffraction argues for increased mobility of inorganic ions accompanying surface ligand desorption. Given previous thermal analysis of $CsPbBr_3$, in which decomposition occurs in a nitrogen atmosphere at temperatures >600 °C,[25] and our own X-ray diffraction data, wholesale decomposition of the inorganic NC material is also not the likely source of irreversible PL loss, although subtle changes in the NC composition due to the increased mobility of ions are possible.

Chemical identification of the thermally reversible trap state is not straightforward from the presented measurements. As excellent ionic conductors with exceptionally fast transport of halides, $CsPbX_3$ materials often have many vacancies.[49,50] The excellent optoelectronic performance of perovskite halides, compared to other halide compounds, has been linked to halide vacancy tolerance arising from the shallow nature of halide vacancy states.[51] $CsPbBr_3$ is the best studied of the samples examined in this work: previous density functional theory (DFT) calculations claim that, within $CsPbBr_3$, bromide vacancies are 0.23[29] or 0.16 eV[51] above the conduction band edge. Nonetheless, these well-known vacancies may be responsible for reversible PL loss at elevated temperatures despite being electronically passive at lower temperatures at which they are not significantly occupied. Reversible, thermally assisted trapping, for a single trap state with energetic barrier E_{trap}, decreases the PL intensity according to Equation (1) Q5: [APT to AU][Please check all equations have been correctly typeset.]

$$I(T) = \frac{I_0}{1 + Ae^{-E_{trap}/kT}} \quad (1)$$

in which A is a parameter related to the cross section of the trap state.[52] At temperatures with kT comparable to the trap energy (and above), substantial PL quenching can occur. Simple thermally assisted trapping of this type should be fully reversible, as opposed to irreversible trapping due to transformation of the material. By fitting the reversible PL loss of the samples (from 80 to 450 K) in Figure 5b, trap barrier heights may be estimated for the $CsPbBr_3$ samples. The results of fitting this temperature regime yield trap activation energies which are mostly consistent with previous DFT calculations (0.16–0.23 eV).[29,51] Estimated barrier heights for $CsPbBr_3$ samples range from 90 to 200 meV (Table S2, Supporting Information). The agreement between predicted trap energies and our experimental data leads us to identify the mechanism of reversible PL loss in $CsPbX_3$ NCs as thermal electron occupation of halogen vacancy centers. Thus, although these materials are remarkably tolerant of halide vacancies, in part because they do not form traps within the band gap, they will still diminish PL intensity with temperature elevation.

4 Conclusion

The temperature dependence of PL was measured for the family of $CsPbX_3$ perovskite NCs with great promise in optoelectronic applications. PL persistence at high temperatures was lower than that of core/shell NCs which have been studied before, but comparable to core-only NCs. Halide composition significantly alters PL intensity above 400 K, with chloride-containing halides showing particularly diminished stability. The samples demonstrate smaller temperature-dependent changes in wavelength than most other semiconductors, including an unusual blueshift with increasing temperature, but also larger temperature-dependent changes in PL broadening, which undermines color purity. Measurements of reversibility, lifetime, and size-dependence implicate thermally assisted trapping, most likely to halogen vacancy centers, as the mechanism of reversible PL loss. These results underscore that although much of the appeal of $CsPbX_3$ NCs rests on their high room-temperature quantum yields due to resilience to defects in the crystal, these defects may play an important role in

diminished performance at higher operating temperatures of optoelectronic devices. Relatively low-temperature irreversible loss observed for these samples also indicates the durability of the strategy of using core/shell structures for enhanced stability.

5 Experimental Section

Materials: Polyvinylbutyral Butvar B-98, oleic acid (90%), oleylamine (70%), octadecene (ODE, 90%), tricotylphosphine (97%), lead bromide (>98%), lead chloride (98%), lead iodide (99%), and cesium carbonate (99.9%) were purchased from Sigma-Aldrich. Oleic acid and oleylamine were dried and stored in a nitrogen filled glovebox. All solvents were ACS grade or higher.

Synthesis: Synthesis of perovskite NCs followed the procedure of Protesescu et al.[6] Typically, a reaction flask containing 4 mL ODE and 0.19 mmol PbX_2 was heated to 120 °C under vacuum and held 1 h. The composition of the lead halide was chosen for a desired output composition of the NCs. Separately, to prepare the Cs-oleate precursor, 407 mg Cs_2CO_3, 1.25 mL oleic acid, and 20 mL ODE were heated under vacuum to 120 °C and held for 1 h, then heated under nitrogen to 150 °C and held until the Cs_2CO_3 completely dissolved. The Cs-oleate precursor was maintained as a homogeneous clear solution by heating prior to injection. Once the reaction flask was under vacuum for 1 h, it was flushed with nitrogen and then 0.5 mL of dry and degassed oleylamine and 0.5 mL of dry and degassed oleic acid were added and the heat was maintained until the reaction flask contained a homogeneous solution. For $CsPbCl_3$ reactions, 1 mL TOP was also added to dissolve $PbCl_2$. Then the reaction flasks were heated under nitrogen flow to 140–170 °C. Upon reaching the set point temperature, 0.4 mL of the Cs-oleate stock solution was rapidly injected. After 5 s, the reaction flasks were cooled with a water bath. Samples were isolated by centrifugation of the NCs.

For temperature-dependent measurements, NCs were diluted into solid films of polyvinylbutyral (Butvar B-98). As reported previously,[16,17] embedding the NCs into a polymer enhanced the NC stability in air. For example, embedded NCs of $CsPbI_3$ exposed to air retained characteristic absorption properties longer than dense thin films of the same sample. Nonetheless, embedding and measurement were performed immediately after synthesis (<24 h). To form dilute polymer films, a 50 mg mL^{-1} chloroform solution of Butvar B-98 was made and then mixed 3:1 with chloroform solution of NCs. According to the manufacturer (Eastman), Butvar B-98 does not show substantial thermal degradation under air or nitrogen until 350 °C, well above the temperatures used in this work. No changes in the polymer films, including evidence of flow or decomposition, were observed during measurements.

Steady-State Measurements: PL measurements were collected using a pulsed 405 nm laser diode directed on to samples of perovskite NCs embedded in polyvinylbutyral, loaded into a variable temperature cryostat/oven. PL was fiber-coupled through a spectrometer to a CCD.

Time-Resolved Optical Measurements: Three kinds of time-resolved measurement were performed in this work. Low-resolution TRPL measurements (≈200 ps) were performed using a pulsed 405 nm laser diode with emission directed on to an avalanche photodiode. Higher time resolution TRPL (≈20 ps) on a streak camera (Hamamatsu) was collected using a 325 nm pulse generated through an optical parametric amplifier using a Ti:sapphire femtosecond laser. TA measurements were performed with the same excitation pulse using a Helios Transient Absorption Spectrometer (Ultrafast Systems).

Thermal Analysis: TGA was performed using a nitrogen purge gas over an aluminum pan containing ≈1 mg dried NCs using a Mettler Toledo TGA. Heating was performed from 25 to 550 °C at 20 °C min^{-1}.

Supporting Information

Supporting Information is available from the Wiley Online Library or from the author.

Acknowledgements

Use of the Center for Nanoscale Materials, an Office of Science user facility, was supported by the U.S. Department of Energy, Office of Science, Office of Basic Energy Sciences, under Contract No. DE-AC02-06CH11357. M.V.K. acknowledges financial support from the European Union through the FP7 (ERC Starting Grant NANOSOLID, GA No. 306733).

1 M. Liu, M. B. Johnston, H. J. Snaith, Nature **2013**, 501, 395.

2 S. A. Veldhuis, P. P. Boix, N. Yantara, M. Li, T. C. Sum, N. Mathews, S. G. Mhaisalkar, Adv. Mater. **2016**, 6804.

Q6: [APT to AU][Please provide the volume number in ref. (2) if applicable.]

3 S. D. Stranks, H. J. Snaith, Nat. Nanotechnol. **2015**, 10, 391.

4 N. K. Noel, S. D. Stranks, A. Abate, C. Wehrenfennig, S. Guarnera, A.-A. Haghighirad, A. Sadhanala, G. E. Eperon, S. K. Pathak, M. B. Johnston, A. Petrozza, L. M. Herz, H. J. Snaith, Energy Environ. Sci. **2014**, 7, 3061.

5 T. C. Jellicoe, J. M. Richter, H. F. J. Glass, M. Tabachnyk, R. Brady, S. E. Dutton, A. Rao, R. H. Friend, D. Credgington, N. C. Greenham, M. L. Böhm, J. Am. Chem. Soc. **2016**, 138, 2941.

6 L. Protesescu, S. Yakunin, M. I. Bodnarchuk, F. Krieg, R. Caputo, C. H. Hendon, R. X. Yang, A. Walsh, M. V. Kovalenko, Nano Lett. **2015**, 15, 3692.

7 D. Fröhlich, K. Heidrich, H. Künzel, G. Trendel, J. Treusch, J. Lumin. **1979**, 18, 385.

8 L. Protesescu, S. Yakunin, M. I. Bodnarchuk, F. Krieg, R. Caputo, C. H. Hendon, R. X. Yang, A. Walsh, M. V. Kovalenko, Nano Lett. **2015**, 15, 3692.

9 S. Yakunin, L. Protesescu, F. Krieg, M. I. Bodnarchuk, G. Nedelcu, M. Humer, G. De Luca, M. Fiebig, W. Heiss, M. V. Kovalenko, Nat. Commun. **2015**, 6, 8056.

10 Y. Wang, X. Li, J. Song, L. Xiao, H. Zeng, H. Sun, Adv. Mater. **2015**, 27, 7101.

11 X. Li, Y. Wu, S. Zhang, B. Cai, Y. Gu, J. Song, H. Zeng, Adv. Funct. Mater. **2016**, 26, 2435.

12 X. Zhang, C. Sun, Y. Zhang, H. Wu, C. Ji, Y. Chuai, P. Wang, S. Wen, C. Zhang, W. W. Yu, J. Phys. Chem. Lett. **2016**, 7, 4602.

13 G. Li, H. Wang, T. Zhang, L. Mi, Y. Zhang, Z. Zhang, W. Zhang, Y. Jiang, Adv. Funct. Mater. **2016**, 26, 8478.

14 E. Yassitepe, Z. Yang, O. Voznyy, Y. Kim, G. Walters, J. A. Castañeda, P. Kanjanaboos, M. Yuan, X. Gong, F. Fan, J. Pan, S. Hoogland, R. Comin, O. M. Bakr, L. A. Padilha, A. F. Nogueira, E. H. Sargent, Adv. Funct. Mater. **2016**, 26, 8757.

15 J. Song, J. Li, X. Li, L. Xu, Y. Dong, H. Zeng, Adv. Mater. **2015**, 27, 7162.

16 M. Meyns, M. Perálvarez, A. Heuer-Jungemann, W. Hertog, M. Ibáñez, R. Nafria, A. Genç, J. Arbiol, M. V. Kovalenko, J. Carreras, A. Cabot, A. G. Kanaras, ACS Appl. Mater. Interfaces **2016**, 8, 19579.

17 Q. Zhou, Z. Bai, W. G. Lu, Y. Wang, B. Zou, H. Zhong, Adv. Mater. **2016**, 28, 9163.

18 C. Sun, Y. Zhang, C. Ruan, C. Yin, X. Wang, Y. Wang, W. W. Yu, Adv. Mater. **2016**, 28, 10088.

19 A. Dualeh, P. Gao, S. I. Seok, M. K. Nazeeruddin, M. Grätzel, Chem. Mater. **2014**, 26, 6160.

20 A. K. Baranwal, S. Kanaya, T. A. N. Peiris, G. Mizuta, T. Nishina, H. Kanda, T. Miyasaka, H. Segawa, S. Ito, ChemSusChem **2016**, 9, 2604.

21 C. Yu, Z. Chen, J. J. Wang, W. Pfenninger, N. Vockic, J. T. Kenney, K. Shum, J. Appl. Phys. **2011**, 110, 063526.

22 F. Zhang, H. Zhong, C. Chen, X. G. Wu, X. Hu, H. Huang, J. Han, B. Zou, Y. Dong, ACS Nano **2015**, 9, 4533.

23 Q. Lü, H. Wei, W. Sun, K. Wang, Z. Gu, J. Li, S. Liu, S. Xiao, Q. Song, Adv. Mater. **2016**, 28, 10165.

24 Y. P. Varshni, Physica **1967**, 34, 149.

25 M. Kulbak, S. Gupta, N. Kedem, I. Levine, T. Bendikov, G. Hodes, D. Cahen, J. Phys. Chem. Lett. **2016**, 7, 167.

26 R. G. Niemann, L. Gouda, J. Hu, S. Tirosh, R. Gottesman, P. J. Cameron, A. Zaban, J. Mater. Chem. A **2016**, 4, 17819.

27 M. Saliba, T. Matsui, J.-Y. Seo, K. Domanski, J.-P. Correa-Baena, M. K. Nazeeruddin, S. M. Zakeeruddin, W. Tress, A. Abate, A. Hagfeldt, M. Grätzel, Energy Environ. Sci. **2016**, 9, 1989.

28 S. Wei, Y. Yang, X. Kang, L. Wang, L. Huang, D. Pan, Chem. Commun. **2016**, 52, 7265.

29 M. Sebastian, J. A. Peters, C. C. Stoumpos, J. Im, S. S. Kostina, Z. Liu, M. G. Kanatzidis, A. J. Freeman, B. W. Wessels, Phys. Rev. B **2015**, 92, 235210.

30 S. Gonzalez-Carrero, R. E. Galian, J. Pérez-Prieto, Opt. Express **2015**, 24, A285.

31 A. Swarnkar, R. Chulliyil, V. K. Ravi, M. Irfanullah, A. Chowdhury, A. Nag, Angew. Chem., Int. Ed. **2015**, 54, 15424.

32 D. Valerini, A. Cretí, M. Lomascolo, L. Manna, R. Cingolani, M. Anni, Phys. Rev. B **2005**, 71, 235409.

33 Z. Li-Gong, S. De-Zhen, F. Xi-Wu, L. Shao-Zhe, Chin. Phys. Lett. **2002**, 19, 578.

34 C. C. Stoumpos, C. D. Malliakas, J. A. Peters, Z. Liu, M. Sebastian, J. Im, T. C. Chasapis, A. C. Wibowo, D. Y. Chung, A. J. Freeman, B. W. Wessels, M. G. Kanatzidis, Cryst. Growth Des. **2013**, 13, 2722.

35 L. Mihut, S. Lefrant, I. Baltog, J. Appl. Phys. **1997**, 82, 5391.

36 B. T. Diroll, C. B. Murray, ACS Nano **2014**, 8, 6466.

37 G. Rainò, T. Stöferle, I. Moreels, R. Gomes, J. S. Kamal, Z. Hens, R. F. Mahrt, G. Raino, T. Stoferle, I. Moreels, R. Gomes, J. S. Kamil, Z. Hens, R. F. Mahrt, ACS Nano **2011**, 5, 4031.

38 P. Jing, J. Zheng, M. Ikezawa, X. Liu, S. Lv, X. Kong, J. Zhao, Y. Masumoto, J. Phys. Chem. C **2009**, 113, 13545.

39 H. Diab, G. Trippé-Allard, F. Lédée, K. Jemli, C. Vilar, G. Bouchez, V. L. R. Jacques, A. Tejeda, J. Even, J.-S. Lauret, E. Deleporte, D. Garrot, J. Phys. Chem. Lett. **2016**, 7, 5093.

40 Y. Zhao, C. Riemersma, F. Pietra, R. Koole, C. de M. Donegá, A. Meijerink, ACS Nano **2012**, 6, 9058.

41 C. E. Rowland, R. D. Schaller, J. Phys. Chem. C **2013**, 117, 17337.

42 L. A. Padilha, J. T. Stewart, R. L. Sandberg, W. K. Bae, W. K. Koh, J. M. Pietryga, V. I. Klimov, Acc. Chem. Res. **2013**, 46, 1261.

43 G. Murtaza, I. Ahmad, Phys. B: Condens. Matter **2011**, 406, 3222.

44 S. Kondo, H. Nakagawa, T. Saito, H. Asada, Curr. Appl. Phys. **2004**, 4, 439.

45 R. Aceves, V. Babin, M. B. Flores, P. Fabeni, A. Maaroos, J. Lumin. **2001**, 93, 27.

46 A. Pan, B. He, X. Fan, Z. Liu, J. J. Urban, A. P. Alivisatos, L. He, Y. Liu, ACS Nano **2016**, 10, 7943.

47 C. E. Rowland, W. Liu, D. C. Hannah, M. K. Y. Chan, D. V. Talapin, R. D. Schaller, ACS Nano **2014**, 8, 977.

48 F. Palazon, F. Di Stasio, S. Lauciello, R. Krahne, M. Prato, L. Manna, J. Mater. Chem. C **2016**, 4, 9179. Q7: [APT to AU][References must be cited in sequential order in the text. Therefore, we have updated the citations and renumbered the reference list accordingly. Please verify.]

49 G. Nedelcu, L. Protesescu, S. Yakunin, M. I. Bodnarchuk, M. J. Grotevent, M. V. Kovalenko, Nano Lett. **2015**, 15, 5635.

50 Q. A. Akkerman, V. D'Innocenzo, S. Accornero, A. Scarpellini, A. Petrozza, M. Prato, L. Manna, J. Am. Chem. Soc. **2015**, 137, 10276.

51 H. Shi, M.-H. Du, Phys. Rev. B **2014**, 90, 174103.

52 D. Bimberg, M. Sondergeld, E. Grobe, Phys. Rev. B **1971**, 4, 3451.